Charge Density Modulation and the Luttinger Liquid State in $MoSe_2$ Mirror Twin Boundaries

Yipu Xia, [†,‡] *Junqiu Zhang,* [†,‡] *Yuanjun Jin,* [†,§] *Wingkin Ho,* [†] *Hu Xu,* [§] *and Maohai Xie* [†,*]

[†]Physics Department, the University of Hong Kong, Pokfulam Road, Hong Kong

[§] Department of Physics, Southern University of Science and Technology, Shenzhen, Guangdong 518055, China

[‡] These authors contributed equally to this work.

[*]Corresponding author. Email: mhxie@hku.hk

ABSTRACT

Mirror twin-domain boundary (MTB) in monolayer $MoSe_2$ represents a (quasi) one-dimensional metallic system. Its electronic properties, particularly the low-energy excitations in the so-called 4|4P-type MTB, have drawn considerable research attention. Reports of quantum well states, charge density waves, and the Tomonaga-Luttinger liquid (TLL) have all been made. Here, by controlling the lengths of the MTBs and employing different substrates, we reveal by low-temperature scanning tunneling microscopy/spectroscopy Friedel oscillations and quantum confinement effect causing the charge density modulations along the defect. The results are inconsistent with charge density waves. Interestingly, for graphene supported samples, TLL in the MTBs is suggested, while that grown on gold, an ordinary Fermi liquid is indicated.

KEYWORDS: 1D metal; mirror twin-domain boundary; quantum well states; Friedel oscillation, Tomonaga-Luttinger liquid

Recently in the studies of monolayer (ML) transition-metal dichalcogenides (TMDs), mirror twin-domain boundaries (MTBs), especially the so-called 4|4P type seen commonly in epitaxial $MoSe_2$, have drawn much attention.[1-4] These defects behave as metals. Being sandwiched between semiconducting pristine TMD domains and supported by insulating or weakly coupled van der Waals (vdW) substrates such as the highly oriented pyrolytic graphite (HOPG) or graphene, these MTBs represent (quasi) one-dimensional (1D) systems exhibiting properties and physics that are pertinent to 1D metals. The density and length of the MTBs are controllable, which have application potentials in chemistry and electronics. Over the past decades, a number of 1D systems

have been intensively studied, including, for example, carbon nanotubes,[5-8] semiconductor nanowires,[9-11] metal chains adsorbed on a semiconductor,[12] nanowire bundles,[13] and quasi-1D organic conductors.[14] Some interesting properties were revealed in these 1D metals. For instance, 1D metals knowingly are prone to the Peierls instability and exhibit a metal-insulator transition, generating charge density waves (CDW) at low-temperature.[15-17] Electron-electron interaction in 1D systems invalidates the Landau description of Fermi liquids and is instead described by the Tomonaga-Luttinger liquid (TLL) theory [18-20] and characterized by properties like spin-charge separation, power-law suppression of electronic density-of-states (DOS) near the Fermi level (E_F),[21-23] modified decay rate of Friedel oscillations [24] *etc.* The TLL has been reportedly observed in various (quasi) 1D systems by transport,[9, 10, 25-27] scanning tunneling spectroscopy,[4, 12, 23, 28, 29] and photoemission spectroscopy [3, 5, 30, 31] studies. For the MTBs in ML $MoSe_2$, TLL was also suggested by a photoemission spectroscopy experiment,[3] whereas a low-temperature scanning tunneling microscopy and spectroscopy (LT-STM/S) study pointed to the Peierls-type CDW.[2] A similar CDW has been suggested in the MTBs formed in $MoTe_2$.[32] On the other hand, Liu *et al.* reported quantum well states (QWS) in finite length MTBs.[1] Jolie *et al.* provided experimental evidences of spin-charge separation and thus the TLL in the so-called 4|4E type MTB in MoS_2.[4] These conflictive results stem partly from the coincidence of the Fermi wave-vector k_F (~1/3a) and the Moiré periodicity (~3a) in the system (*i.e.*, $MoSe_2$-on-graphene) and that the QWS and CDW both give rise to energy gaps at E_F . Indeed, MTBs in as-grown $MoSe_2$ are usually short, so quantum confinement effect can always be prominent, making the identification of QWS against CDW difficult in experiments.

In this work, we present a detailed room-temperature (RT) and LT-STM/S study of the common 4|4P type MTBs in $MoSe_2$ with changing lengths and grown on different substrates by molecular-

beam epitaxy (MBE). Networks of the 4|4P-MTBs form readily in epitaxial $MoSe_2$ ML and their density is tunable by changing the MBE conditions.[33] As a result, MTBs of varying lengths and densities are achieved, making it possible to study the phenomena and physics of 1D metals. By examining the electronic properties of such defects of varying lengths at low temperatures (~5 K and 77 K), we show evidence of Friedel oscillation, the QWS and the TLL for HOPG/graphene supported samples. The MTBs in Au-supported samples conform to the ordinary Fermi liquid behavior while the QWS remains conspicuous in finite length defects. Charge density modulations along the MTBs are observable even at RT, suggesting that they are unlikely associated with CDW.

RESULTS AND DISCUSSIONS

Atomic and Electronic Structures of 4|4P-MTBs. Fig. 1a presents an STM image of an epitaxial $MoSe_2$ ML grown on graphene, revealing a dense MTB network with each MTB segment approximately 5 nm long. The density and length of the MTBs are controllable by changing the MBE condition or by performing post-growth annealing. For example, upon annealing the sample of Fig. 1a at ~700℃ for 1 hour, more isolated and longer MTBs are obtained (see Fig. 1b). Surrounding each MTB defect are two semiconducting $MoSe_2$ domains having a bandgap of ~2.1 eV as measured by STS.[1, 34, 35] The atomic structure of the defect has already been established (Fig. 1c) and the corresponding electronic structure as calculated from the density functional theory (DFT) is shown in Fig. 1d.[36, 37] In the latter, we have upshifted the Fermi level to a value that matches with our experiment,[2] *i.e.*, at $k \approx 0.36$ Å^{-1}. The dispersions labeled '1' and '2' (red color) in the gap region of pristine $MoSe_2$ ML are from the MTB, signifying the metallic property of the 1D defect. The simplicity of the band structure near the Fermi level makes the MTB an ideal

system for studying properties related to the dimensionality, electron interaction and quantum confinement effect, *etc.*

Quantum Well States in Finite-Length MTBs. In Fig. 2a, we show a set of STS spectra taken on the MTBs of different lengths, revealing a prominent feature of gap opening at the Fermi level E_F. The size of the energy gap E_g increases with decreasing MTB length *L*. Fig. 2b summarizes the data collected from a number of defects with lengths ranging from 3.1 nm to 40.7 nm and measured by STS at ~5 K. As seen, the data can be reasonably fitted by $E_g \sim 1/L$ (solid line). The latter is one of the signatures of the TLL as will be discussed below. For now, we draw attention of another, albeit less apparent, feature in the spectra, *i.e.*, a periodic variation of the DOS with energy (visible in the top spectrum in Fig. 2a), signifying the QWS due to finite length of the defects. The QWS is best visualized by the color plot of Fig. 2c which shows the measured $\frac{dI}{dV}$ as functions of energy (vertical axis) and position (horizontal) along the MTB. Spatial modulations of the charge density as well as energy quantization are clearly discerned. The number of modulation periods increases with energy, from 4 (at about -0.26 eV) to 7 (around +0.18 eV). This appears consistent with the dispersion of the defect-band '1' in Fig. 1c. At energy ~0.2 eV, a much enhanced intensity is noted, which corresponds to the emergence of band '2'. Above 0.2 eV, there are degenerate states due to the overlapping bands '1' and '2', complicating the data.

Consistent with Fig. 2a, a much wider energy gap than the expected QWS gap is observed at the Fermi level (0 eV). This extra gap at E_F may be attributed to a Coulomb blockade effect, or the charge-gap, of the TLL.[4, 19] Indeed, interacting electrons in 1D behave as the TLL, and if confined in finite lengths, not only their energies become quantized, but also that a zero-mode gap is created

at Fermi level due to Coulomb blockade. This zero-mode gap has been found to be inversely proportional to L,[4, 19] which describes well our experimental data of Fig. 2b.

The assignment that electrons in MTBs are TLL in the graphene-supported samples implies strong electron-electron interaction in the MTBs and a weak coupling with the graphene (and HOPG) substrate. The latter has been indicated by some previous theoretical investigations.[38, 39] If, on the other hand, tunneling of electrons between MTBs and the substrate is significant or electron-electron interaction becomes suppressed due to, *e.g.*, the screening effect, the MTBs would no longer behave as the TLL. For comparison, we have grown a $MoSe_2$ film on Au(110) substrate, in which MTBs are also seen as exemplified in Figs. 3a and 3b. Spatially-resolved STS spectra of such a MTB is presented in Fig. 3c, in which the QWS are again clearly discerned. Hence, the QWS in finite-length MTBs are unequivocal irrespective of the substrates used, HOPG/graphene or Au(110).

Comparing Fig. 3c and Fig. 2c, an acute feature is however noted, *i.e.*, it lacks the extra gap at E_F in Fig. 3c. This indicates that the MTB in the gold-supported sample does not behave as the TLL but a Fermi liquid, a striking effect of the substrate. Though the precise nature of it remains unclear, two factors are believed to be relevant. The first is electronic coupling between the MTBs and substrates. On graphene, some early theoretical studies indicated weak couplings between $MoSe_2$ and the substrate,[38, 39] so the MTBs in $MoSe_2$ would behave more like 1D metals. On Au, on the other hand, due to a different nature of interface interaction, tunneling of electrons between the MTB and the substrate may be substantial, and if so the MTBs would no longer represent 1D

systems. The second and perhaps a more relevant factor is the screening effect as demonstrated previously in single-wall carbon nanotubes, where electron-electron interaction became suppressed by screening from the metallic substrates.[8, 25, 26, 40, 41] On graphene, the screening effect is minimal due to a low density of electrons in graphene, whereas on Au, the high density of electrons in the substrate can provide strong screening and thus effectively suppresses electron-electron interaction in the MTBs. This would in turn diminish the TLL and lead to the Fermi liquid in the MTBs. This, in passing, would also provide a strong hint that the Peierls type CDW is not relevant here, as the latter is of the single-particle phenomenon and would not exhibit such a substrate dependence due to screening. We shall return to a further discussion of the CDW in a later subsection, but the essential point made here is that the QWS is conspicuous in finite-length MTBs on both graphene, HOPG, and Au, though different substrates may have changed the character of the quasi particle from the TLL to a Fermi liquid depending on the strength of the coupling and/or screening effects.

TLL in Graphene/HOPG-Supported MTBs. As noted above, MTBs in graphene/HOPG-supported $MoSe_2$ ML behave as the TLL. This is further evidenced by the observation of a power-law suppression of the DOS at E_F for long defects (*e.g.*, > 30 nm) where quantum effect becomes insignificant. Indeed, for long MTBs, we could hardly observe the charge-gap at E_F, nor the QWS. Instead, the measured spectra exhibit an apparent power-law suppression of the DOS close to the Fermi level, another feature characteristic of the TLL.[18, 42-45] As an example, Fig. 4a presents a spectrum taken at ~5K over a MTB segment of over 35 nm long, and Fig. 4b presents a close-up spectrum near the Fermi energy. As seen, instead of a gap, a power-law suppression of the DOS, $N(E) \propto \frac{\mathrm{d}I}{\mathrm{d}V}$, may be observed over a substantial energy range of ~300 meV, and a fit by

$N(E) \sim |E|^{\alpha}$ results in an exponent $\alpha = 0.47 \pm 0.05$. As the temperature is increased to ~77K, the d*I*/d*V* spectrum preserves the same power-law behavior but features a reduced DOS suppression at zero-bias (Fig. 4c). Such a behavior agrees with the TLL model description of $N(E) \sim T^{\alpha}$ and has been observed in many TLL systems.[12, 25, 46] The power-law exponent relates to the Luttinger parameter K_c according to $\alpha = \left(K_c + K_c^{-1} - 2\right)/4$,[19, 44, 47] which characterizes the strength of electron-electron interactions in the system. From the above, we derive a value of $K_c \approx 0.28$. We note further that the power-law suppression is consistently observed even if the tip-to-sample distance is changed in the STS measurements.

Besides DOS suppression at Fermi level, an additional feature that may lend support to the TLL in graphene-supported MTBs is the DOS peak upshift in energy with decreasing *r*, the distance from the 1D wire edge, such that $r \times E$ = constant.[44, 45] Fig. 5a presents a spatially-resolved STS spectra taken from an isolated MTB but near one end terminated at the ML-$MoSe_2$ island edge. A curve of $r \times E = 0.49$ nm·eV is overlaid in the figure. Fig. 5b plots the same data in a different format, where each line represents a spectrum taken at a location a distance from one of the MTB ends as indicated. As is clear, the closer it is to the end of the defect, the higher the energy at which the DOS is the highest, consistent with the TLL.

Charge Density Modulation – the QWS, Friedel Oscillation, Moiré and CDW. A feature in all STM measurements of the MTBs is the apparent intensity modulations with period ~3*a*, *i.e.*, triple the lattice constant of $MoSe_2$ along the defect. While an early study attributed such modulations to the QWS and Moiré potentials,[1] others suggested them to reflect the CDW.[2, 48] As pointed out before, the difficulty in identifying the true origin of such STM intensity modulation

lies in the coincidence of the Fermi wave-vector k_F with the inverse of the Moiré periodicity (~3a) for $MoSe_2$-on-graphene. Meanwhile, both QWS and CDW give rise to energy gaps at E_F. Scattering by defects or the intersections of the MTBs can also lead to charge modulations per the interference of the scattered electron waves. In below, we shall show evidence that the charge density modulations of period ~3a is more related to the QWS or interference effect rather than Moiré and the CDW.

As already mentioned, a 1D metal is unstable at LT against Peierls transition, where lattice distortion leads to a gap opening at E_F, giving rise to charge density waves of wave-vector ~2k_F. The gap size depends on the strength of electron-electron interaction, which determines the temperature of CDW transition. In a previous study, a CDW gap of ~0.1 eV was suggested in the MTBs in $MoSe_2$ ML,[2] which implies a transition temperature of ~200 K as was subsequently observed by transport measurements.[3] We have however performed STM measurements at RT, an example of which is shown in Fig. 6a. Intensity modulations of period ~0.93 nm remains visible, which is thus inconsistent with the early prediction of the CDW transition at ~200 K. In fact, looking at the MTBs in Au(110)-supported $MoSe_2$ (Fig. 3), careful measurement of the modulation period shows a bias dependence: it is in average ~1.17 nm when imaged at -0.1 V but ~1.10 nm at +0.1 V. If it were CDW, the same modulation period would be expected but with a phase shift of π.[2] We note further that in MTBs supported on Au(110), no Moiré pattern is present, so the effect of Moiré potential may also be ruled out as the cause of the observed charge density modulations.

An additional feature that does not align well with the CDW is the length-dependent energy gap at E_F as presented in Fig. 2b. Indeed, gap opening at E_F may be taken as one of the signatures of CDW formation, though there also are cases where CDW does not necessarily lead to energy gaps, especially in higher dimensional systems.[49, 50] If however a gap does open as shown in the

cases of finite-length MTBs, the gap size would be constant rather than inversely length-dependent. Besides, for long MTBs, we failed to measure the DOS gaps but only a suppression at the Fermi level (see Fig. 4). These findings are all inconsistent with the CDW. We have in fact performed some DFT calculations by, *e.g.*, artificially distorting the regular MTB structure (Fig. 1c) to introduce the 3*a* periodicity by compressing every three-unit cell by 5 pm, 10 pm or 15 pm, respectively. After relaxation, all returned to the undistorted structure, which agrees with others [2] and suggests that the distorted lattices are not stable. As a matter of fact, MTBs in $MoSe_2$ are not exactly 1D metals of the Peierls model. While electrons are very much confined to 1D along the MTBs, the lattice extends in two-dimensions where atoms in the MTB core are bonded covalently with the neighboring $MoSe_2$. So the phononic system is two-dimensional, and any lattice distortion along the MTB inevitably results in stresses in the whole $MoSe_2$ lattice with huge strain energies. It is therefore not surprising for the system not to exhibit the Peierls instability. With this said, we however wish to point out that CDW may form without invoking lattice distortions but by other effects due to electron interactions *via*, *e.g.*, the Overhauser mechanism.[50-53] Indeed in a recent DFT study by incorporating a Hubbard potential in the MTBs, spin and charge density waves have been suggested.[48] The point we wish to make is that for the MTBs in ML-$MoSe_2$, our STM data, including RT-STM, bias-dependent modulation periods, lack of energy gap in long MTBs but length-dependent gaps for short MTBs, as well as the substrate effect elaborated earlier, all point to inconsistencies with the CDW. The charge density modulations seen in experiments are better explained by the quantum confinement and interference effects as discussed below.

Indeed, as presented earlier, QWS are ubiquitous in finite-length MTBs supported on both graphene and Au(110) substrates. The QWS inevitably causes charge density modulations. During imaging at low bias, the STM contrast comes predominantly from states close to the Fermi energy,

and the modulation period will thus not far from that of $1/k_F$. Comparing the MTBs on Au(110) *versus* that on graphene/HOPG, we note the modulation periods are slightly different, *i.e*, ~1.12 nm on Au and ~0.93 nm on graphene/HOPG by averaging over many STM measurements. This may be explained by a relative Fermi level shift between the two samples due to work-function and DOS differences. Often, especially in long MTBs, we observe STM intensity modulations of non-uniform amplitudes along the defect. Examples are shown in Fig. 6b and 6c for the MTBs on HOPG and Au(110), respectively, where the modulations are seen to be the strongest near the defect or edge of the MTB and decrease gradually as one moves away. This behavior is describable by the Friedel oscillations. For that on Au, which is a Fermi liquid as discussed earlier, the intensity is found to decay per the relation of $\rho \sim 1/x$,[54, 55] while for the MTB on graphene/HOPG, it is TLL and the modulation amplitude decays at a slower rate according to $\rho \sim x^{-K_C}$, where K_C is the Luttinger parameter.[24] The insets in Figs. 6b and 6c show plots of such relations with K_C = 0.28 being chosen in Fig. 6b per the result of Fig. 3, showing the satisfactory agreements.

CONCLUSION

We use RT- and LT-STM/S to reveal that the commonly observed 4|4P type MTBs in epitaxial $MoSe_2$ ML host quantum well states, which is the dominant factor for the observed intensity modulations in STM micrographs. For graphene/HOPG supported samples, signatures of Tomonaga-Luttinger liquid are observed, which include the opening of the charge gaps at the Fermi level for short MTBs and the power-law DOS suppression in long MTBs. The former shows an inverse relation with MTB length. Friedel oscillations close to the MTB edge and/or defects also conform to the TLL in graphene/HOPG supported samples. On Au(110), MTBs behave as

Fermi liquids. In any case, CDW is not evident by our RT-STM measurements and by comparing results between samples grown on graphene/HOPG and Au(110) substrates. The effect of Moiré potential is also ruled out. The data suggest the important role of interface interaction between the MTBs and substrates, *e.g.*, by the tunneling and screening effects, in determining the electronic properties of the MTBs. It provides an interesting 1D system for studying low-dimensional and correlated physics.

METHODS

Sample Preparations. Depositions of ML $MoSe_2$ were carried out in an MBE chamber having the background pressure of 10^{-10} Torr. The flux of molybdenum was generated from an e-beam evaporator operated at a power of ~50 W, and that of selenium was delivered by a Knudsen cell held at 125℃. For the depositions on vdW substrates, HOPG or epitaxial graphene obtained by annealing SiC wafer at ~1100℃ in a Si flux were used. The temperature of the substrate during growth was ~500℃. The growth rate was about 0.5 MLs/hr as limited by the flux of Mo (~1.5×10^{11} atoms/cm^2·s), which was about 10 times lower than Se flux (~1.2×10^{12} molecules/cm^2·s). The growing surface was monitored by reflection high-energy electron diffraction (RHEED) operated at 15 keV. Upon completion of ~ 1 ML $MoSe_2$ deposition, the film was capped by an amorphous Se layer deposited at room-temperature, where the streaky RHEED patterns of $MoSe_2$ changed into diffusive one. It was then taken out of the MBE chamber and transferred to a standalone Unisoku 1500 STM system, in which a post-growth annealing procedure was adopted at 700℃ for 1 hour to desorb the Se capping layer as well as to tune the density and thus the length of twin domain boundary defects in $MoSe_2$. For deposition of ML $MoSe_2$ on crystalline Au(110), the substrate was cleaned by Ar^+ bombardment (1.0 keV, 3×10^{-6} Torr), followed by annealing at

~600℃. It was then transferred into the adjacent MBE chamber for $MoSe_2$ growth. The deposition conditions were the same as described above, so was the procedure for subsequent STM measurements.

Characterizations. Subsequent STM/STS measurements were carried out at 77K or 5K under a base pressure 1×10^{-10} Torr. The constant-current mode of scanning was adopted, and the tunneling current was 100pA. The d*I*/d*V* spectra were obtained by a lock-in amplifier at 1.009 kHz. Tungsten tips calibrated on single-crystal Ag(111) surface were used for the scanning. Room temperature STM measurement were done in an Omicron STM system under a base pressure 3×10^{-10} Torr.

DFT Calculations. The first-principles calculations were performed by using the density functional theory (DFT) as coded in the Vienna *ab initio* simulation package (VASP). The projector augmented wave (PAW) method was used to describe the electron core interactions with the cutoff energy 500 eV. The Perdew-Burke-Ernzerhof (PBE) formalism of generalized gradient approximation (GGA) was applied to treat the exchange-correlation, and the BZ was sampled by a *k*-point mesh 11 × 1 × 1 in the self-consistency cycle.

ASSOCIATED CONTENT

The authors declare no competing financial interest.

AUTHOR INFORMATION

Corresponding Authors

* Email: mhxie@hku.hk (MHX).

Author Contributions

M.X. conceived and coordinated this work. Y.X. and J.Z. performed the MBE growth and STM/S experiments. Y.J. carried out the theoretical calculations with the supervision from H.X. W.H. provided technical support and participated in the discussions. Y.X. and J.Z contributed equally to this work.

ACKNOWLEDGEMENTS

We benefitted from discussions with C.J. Wang, W. Yao and H.L. Yu. H.J Liu and L. Jiao help with some RT-STM measurements. The work is supported by a Collaborative Research Grant (No. C7036-17W) and a General Research Grant (17327316) from the Research Grant Council of Hong Kong Special Administrative Region, China.

REFERENCES

1. Liu, H.; Jiao, L.; Yang, F.; Cai, Y.; Wu, X.; Ho, W.; Gao, C.; Jia, J.; Wang, N.; Fan, H.; Yao, W.; Xie, M. H., Dense Network of One-Dimensional Midgap Metallic Modes in Monolayer $MoSe_2$ and Their Spatial Undulations. *Phys. Rev. Lett.* **2014,** *113*, 066105.

2. Barja, S.; Wickenburg, S.; Liu, Z.-F.; Zhang, Y.; Ryu, H.; Ugeda, M. M.; Hussain, Z.; Shen, Z.-X.; Mo, S.-K.; Wong, E.; Salmeron M. B.; Wang F.; Crommie, M. F.; Ogletree D. F.; Neaton, J. B.; Weber-Bargioni, A., Charge Density Wave Order in 1D Mirror Twin Boundaries of Single-Layer $MoSe_2$. *Nat. Phys.* **2016,** *12*, 751.

3. Ma, Y.; Diaz, H. C.; Avila, J.; Chen, C.; Kalappattil, V.; Das, R.; Phan, M.-H.; Čadež, T.; Carmelo, J. M.; Asensio, M. C.; Batzill, M., Angle Resolved Photoemission Spectroscopy Reveals Spin Charge Separation in Metallic $MoSe_2$ Grain Boundary. *Nat. Commun.* **2017,** *8*, 14231.

4. Jolie, W.; Murray, C.; Weiß, P. S.; Hall, J.; Portner, F.; Atodiresei, N.; Krasheninnikov, A. V.; Busse, C.; Komsa, H.-P.; Rosch, A.; Michely, T., Tomonaga-Luttinger Liquid in a Box: Electrons Confined within MoS_2 Mirror-Twin Boundaries. *Phys. Rev. X* **2019,** *9*, 011055.

5. Ishii, H.; Kataura, H.; Shiozawa, H.; Yoshioka, H.; Otsubo, H.; Takayama, Y.; Miyahara, T.; Suzuki, S.; Achiba, Y.; Nakatake, M.; Narimura, T.; Higashiguchi, M.; Shimada, K.; Namatame, H.; Taniguchi, M., Direct Observation of Tomonaga–Luttinger-Liquid State in Carbon Nanotubes at Low Temperatures. *Nature* **2003,** *426*, 540.

6. Egger, R.; Gogolin, A. O., Effective Low-Energy Theory for Correlated Carbon Nanotubes. *Phys. Rev. Lett.* **1997,** *79*, 5082.

7. Kane, C.; Balents, L.; Fisher, M. P., Coulomb Interactions and Mesoscopic Effects in Carbon Nanotubes. *Phys. Rev. Lett.* **1997,** *79*, 5086.

8. Yao, Z.; Postma, H. W. C.; Balents, L.; Dekker, C., Carbon Nanotube Intramolecular Junctions. *Nature* **1999,** *402*, 273.

9. Auslaender, O.; Steinberg, H.; Yacoby, A.; Tserkovnyak, Y.; Halperin, B.; Baldwin, K.; Pfeiffer, L.; West, K., Spin-Charge Separation and Localization in One Dimension. *Science* **2005,** *308*, 88-92.

10. Jompol, Y.; Ford, C.; Griffiths, J.; Farrer, I.; Jones, G.; Anderson, D.; Ritchie, D.; Silk, T.; Schofield, A., Probing Spin-Charge Separation in a Tomonaga-Luttinger Liquid. *Science* **2009,** *325*, 597-601.

11. Yacoby, A.; Stormer, H.; Wingreen, N. S.; Pfeiffer, L.; Baldwin, K.; West, K., Nonuniversal

Conductance Quantization in Quantum Wires. *Phys. Rev. Lett.* **1996,** *77*, 4612.

12. Blumenstein, C.; Schäfer, J.; Mietke, S.; Meyer, S.; Dollinger, A.; Lochner, M.; Cui, X.; Patthey, L.; Matzdorf, R.; Claessen, R., Atomically Controlled Quantum Chains Hosting a Tomonaga–Luttinger Liquid. *Nat. Phys.* **2011,** *7*, 776.

13. Venkataraman, L.; Hong, Y. S.; Kim, P., Electron Transport in a Multichannel One-Dimensional Conductor: Molybdenum Selenide Nanowires. *Phys. Rev. Lett.* **2006,** *96*, 076601.

14. Claessen, R.; Sing, M.; Schwingenschlögl, U.; Blaha, P.; Dressel, M.; Jacobsen, C. S., Spectroscopic Signatures of Spin-Charge Separation in the Quasi-One-Dimensional Organic Conductor Ttf-Tcnq. *Phys. Rev. Lett.* **2002,** *88*, 096402.

15. Yeom, H. W.; Takeda, S.; Rotenberg, E.; Matsuda, I.; Horikoshi, K.; Schaefer, J.; Lee, C.; Kevan, S.; Ohta, T.; Nagao, T.; Hasegawa; S., Instability and Charge Density Wave of Metallic Quantum Chains on a Silicon Surface. *Phys. Rev. Lett.* **1999,** *82*, 4898.

16. Ahn, J.; Byun, J.; Koh, H.; Rotenberg, E.; Kevan, S.; Yeom, H., Mechanism of Gap Opening in a Triple-Band Peierls System: In Atomic Wires on Si. *Phys. Rev. Lett.* **2004,** *93*, 106401.

17. Ahn, J. R.; Yeom, H. W.; Yoon, H. S.; Lyo, I. W., Metal-Insulator Transition in Au Atomic Chains on Si with Two Proximal Bands. *Phys. Rev. Lett.* **2003,** *91*, 196403.

18. Luttinger, J., Fermi Surface and Some Simple Equilibrium Properties of a System of Interacting Fermions. *Phys. Rev.* **1960,** *119*, 1153.

19. Voit, J., One-Dimensional Fermi Liquids. *Rep. Prog. Phys.* **1995,** *58*, 977.

20. Tomonaga, S.-i., Remarks on Bloch's Method of Sound Waves Applied to Many-Fermion Problems. *Prog. Theor. Phys.* **1950,** *5*, 544-569.

21. Mattsson, A. E.; Eggert, S.; Johannesson, H., Properties of a Luttinger Liquid with Boundaries at Finite Temperature and Size. *Phys. Rev. B* **1997,** *56*, 15615-15628.

22. Kane, C. L.; Fisher, M. P., Transport in a One-Channel Luttinger Liquid. *Phys. Rev. Lett.* **1992,** *68*, 1220-1223.

23. Xia, Y.; Wang, B.; Zhang, J.; Jin, Y.; Tian, H.; Ho, W.; Xu, H.; Jin, C.; Xie, M. H., Quantum Confined Tomonaga–Luttinger Liquid in Mo_6Se_6 Nanowires Converted from an Epitaxial $MoSe_2$ Monolayer. *Nano Lett.* **2020,** *20*, 2094-2099.

24. Egger, R.; Grabert, H., Friedel Oscillations for Interacting Fermions in One Dimension. *Phys. Rev. Lett.* **1995,** *75*, 3505.

25. Bockrath, M.; Cobden, D. H.; Lu, J.; Rinzler, A. G.; Smalley, R. E.; Balents, L.; McEuen, P. L., Luttinger-Liquid Behaviour in Carbon Nanotubes. *Nature* **1999,** *397*, 598-601.

26. Gao, B.; Komnik, A.; Egger, R.; Glattli, D. C.; Bachtold, A., Evidence for Luttinger-Liquid Behavior in Crossed Metallic Single-Wall Nanotubes. *Phys. Rev. Lett.* **2004,** *92*, 216804.

27. Hashisaka, M.; Hiyama, N.; Akiho, T.; Muraki, K.; Fujisawa, T., Waveform Measurement of Charge- and Spin-Density Wavepackets in a Chiral Tomonaga–Luttinger Liquid. *Nat. Phys.* **2017,** *13*, 559.

28. Hager, J.; Matzdorf, R.; He, J.; Jin, R.; Mandrus, D.; Cazalilla, M.; Plummer, E. W., Non-Fermi-Liquid Behavior in Quasi-One-Dimensional $Li_{0.9}Mo_6O_{17}$. *Phys. Rev. Lett.* **2005,** *95*, 186402.

29. Wang, F.; Alvarez, J.; Mo, S.-K.; Allen, J.; Gweon, G.-H.; He, J.; Jin, R.; Mandrus, D.; Höchst, H., New Luttinger-Liquid Physics from Photoemission on $Li_{0.9}Mo_6O_{17}$. *Phys. Rev. Lett.* **2006,** *96*, 196403.

30. Segovia, P.; Purdie, D.; Hengsberger, M.; Baer, Y., Observation of Spin and Charge Collective Modes in One-Dimensional Metallic Chains. *Nature* **1999,** *402*, 504.

31. Ohtsubo, Y.; Kishi, J.-i.; Hagiwara, K.; Le Fèvre, P.; Bertran, F.; Taleb-Ibrahimi, A.; Yamane, H.; Ideta, S.-i.; Matsunami, M.; Tanaka, K.; Kimura S., Surface Tomonaga-Luttinger-

Liquid State on Bi/InSb(001). *Phys. Rev. Lett.* **2015,** *115*, 256404.

32. Wang, L.; Wu, Y.; Yu, Y.; Chen, A.; Li, H.; Ren, W.; Lu, S.; Ding, S.; Yang, H.; Xue, Q.-K.; Li, F.; Wang, G., Direct Observation of One-Dimensional Peierls-Type Charge Density Wave in Twin Boundaries of Monolayer $MoTe_2$. *ACS Nano* **2020**, 14, 8299-8306.

33. Jiao, L.; Liu, H. J.; Chen, J.; Yi, Y.; Chen, W.; Cai, Y.; Wang, J.; Dai, X.; Wang, N.; Ho, W. K.; Xie, M. H., Molecular-Beam Epitaxy of Monolayer $MoSe_2$: Growth Characteristics and Domain Boundary Formation. *New J. Phys.* **2015,** *17*, 053023.

34. Xia, Y.; Wang, B.; Zhang, J.; Feng, Y.; Li, B.; Ren, X.; Tian, H.; Xu, J.; Ho, W.; Xu, H.; Liu, C.; Jin, C.; Xie, M. H., Hole Doping in Epitaxial $MoSe_2$ Monolayer by Nitrogen Plasma Treatment. *2D Mater.* **2018,** *5*, 041005.

35. Xia, Y.; Zhang, J.; Yu, Z.; Jin, Y.; Tian, H.; Feng, Y.; Li, B.; Ho, W.; Liu, C.; Xu, H.; Jin, C.; Xie, M. H., A Shallow Acceptor of Phosphorous Doped in $MoSe_2$ Monolayer. *Adv. Electron. Mater.* **2020,** *6*, 1900830.

36. Böker, T.; Severin, R.; Müller, A.; Janowitz, C.; Manzke, R.; Voß, D.; Krüger, P.; Mazur, A.; Pollmann, J., Band Structure of MoS_2, $MoSe_2$, and α-$MoTe_2$: Angle-Resolved Photoelectron Spectroscopy and *Ab Initio* Calculations. *Phys. Rev. B* **2001,** *64*, 235305.

37. Hong, J.; Wang, C.; Liu, H.; Ren, X.; Chen, J.; Wang, G.; Jia, J.; Xie, M. H.; Jin, C.; Ji, W.; Yuan, J.; Zhang, Z., Inversion Domain Boundary Induced Stacking and Bandstructure Diversity in Bilayer $MoSe_2$. *Nano Lett.* **2017,** *17*, 6653-6660.

38. Komsa, H.-P.; Krasheninnikov, A. V., Electronic Structures and Optical Properties of Realistic Transition Metal Dichalcogenide Heterostructures from First Principles. *Phys. Rev. B* **2013,** *88*, 085318.

39. Sachs, B.; Britnell, L.; Wehling, T. O.; Eckmann, A.; Jalil, R.; Belle, B. D.; Lichtenstein,

A. I.; Katsnelson, M. I.; Novoselov, K. S., Doping Mechanisms in Graphene-MoS_2 Hybrids. *Appl. Phys. Lett.* **2013,** *103*, 251607.

40. Kakashvili, P.; Johannesson, H.; Eggert, S., Local Spectral Weight of a Luttinger Liquid: Effects from Edges and Impurities. *Phys. Rev. B* **2006,** *74*, 085114.

41. Hashisaka, M.; Fujisawa, T., Tomonaga-Luttinger-Liquid Nature of Edge Excitations in Integer Quantum Hall Edge Channels. *Rev. Phys.* **2018,** *3*, 32-43.

42. Meden, V.; Metzner, W.; Schollwöck, U.; Schneider, O.; Stauber, T.; Schönhammer, K., Luttinger Liquids with Boundaries: Power-Laws and Energy Scales. *Eur. Phys. J. B* **2000,** *16*, 631-646.

43. Voit, J., Charge-Spin Separation and the Spectral Properties of Luttinger Liquids. *J. Phys.: Condens. Matter* **1993,** *5*, 8305.

44. Eggert, S., Scanning Tunneling Microscopy of a Luttinger Liquid. *Phys. Rev. Lett.* **2000,** *84*, 4413-6.

45. Lee, J.; Eggert, S.; Kim, H.; Kahng, S.-J.; Shinohara, H.; Kuk, Y., Real Space Imaging of One-Dimensional Standing Waves: Direct Evidence for a Luttinger Liquid. *Phys. Rev. Lett.* **2004,** *93*, 166403.

46. Stühler, R.; Reis, F.; Müller, T.; Helbig, T.; Schwemmer, T.; Thomale, R.; Schäfer, J.; Claessen, R., Tomonaga-Luttinger Liquid in the Edge Channels of a Quantum Spin Hall Insulator. *Nat. Phys.* **2020,** *16*, 47-51.

47. Schulz, H., Correlation Exponents and the Metal-Insulator Transition in the One-Dimensional Hubbard Model. *Phys. Rev. Lett.* **1990,** *64*, 2831.

48. Krishnamurthi, S.; Brocks, G., The Sign of Three: Spin/Charge Density Waves at the Boundaries of Transition Metal Dichalcogenides. **2020**, *arXiv: Materials Science/2005.02519.*

arXiv.rog e-Print archive. https://arxiv.org/abs/2005.02519 (accessed Jul 31, 2020).

49. Barnett, R. L.; Polkovnikov, A.; Demler, E.; Yin, W.-G.; Ku, W., Coexistence of Gapless Excitations and Commensurate Charge-Density Wave in the *2H* Transition Metal Dichalcogenides. *Phys. Rev. Lett.* **2006,** *96*, 026406.

50. Zhu, X.; Guo, J.; Zhang, J.; Plummer, E., Misconceptions Associated with the Origin of Charge Density Waves. *Adv. Phys. : X* **2017,** *2*, 622-640.

51. Overhauser, A., Observability of Charge-Density Waves by Neutron Diffraction. *Phys. Rev. B* **1971,** *3*, 3173.

52. Overhauser, A., Photoemission from the Charge-Density Wave in Na and K. *Phys. Rev. Lett.* **1985,** *55*, 1916.

53. Zhu, X.; Cao, Y.; Zhang, J.; Plummer, E.; Guo, J., Classification of Charge Density Waves Based on Their Nature. *Proc. Natl. Acad. Sci.* **2015,** *112*, 2367-2371.

54. Friedel, J., Metallic Alloys. *Nuovo Cim.* **1958,** *7*, 287-311.

55. Tütto, I.; Zawadowski, A., Quantum Theory of Local Perturbation of the Charge-Density Wave by an Impurity: Friedel Oscillations. *Phys. Rev. B* **1985,** *32*, 2449.

FIGURE CAPTIONS:

Figure. 1. Atomic and electronic structures of MTBs in $MoSe_2$. (a) STM image (image size: 15 × 10 nm^2, sample bias: +0.4 V) showing the triangular network of MTBs (bright contrast double lines) in an MBE-grown $MoSe_2$ ML. (b) STM image (image size: 30 × 20 nm^2, sample bias: −1.0 V) showing MTBs in a post-annealed $MoSe_2$ ML. (c) Stick-and-ball model of a MTB in $MoSe_2$ (top and side view), where purple and green balls represent Mo and Se atoms respectively. (d) DFT calculated band structure, where states (*e.g.*, '1' and '2') of the MTB are highlighted in red. Black and light-blue lines are states from the bulk and edges of $MoSe_2$ ML ribbon, respectively.

Figure. 2. Quantum well states in finite length MTBs. (a) STS spectra ($\frac{dI}{dV}$ on a logarithmic scale) taken from the MTBs of three different lengths as indicated. (b) The DOS gap at Fermi level measured by STS as function of MTB lengths. The red line represents a least-square fitting by $E_g \sim 1/L$. (c) Spatially-resolved STS spectra of a MTB of total length ~7 nm but measured for a length of ~5 nm in the middle.

Figure. 3. MTB in $MoSe_2$ ML grown on Au(110). (a-b) STM images (sizes: 14 × 14 nm^2) of a MTB loop acquired at the sample bias of (a) +0.1 V and (b) −0.1 V. (c) Spatially-resolved STS spectra of a MTB of total length ~10 nm but measured for a length of ~7 nm in the middle region.

Figure. 4. DOS power-law suppression at E_F in long MTBs. (a) a STS spectrum obtained under ~5K from a MTB of total length ~35 nm. (b) A close-up view of (a) over a narrow energy range. The red line represents a fit of the data by the power-law $N(E) \sim |E|^{\alpha}$ with an exponent $\alpha = 0.47$. (c) A STS spectrum measured under ~77K.

Figure. 5. DOS peak energy as a function of tip position. (a) spatially-resolved STS taken near one end (defined as the origin) of a MTB, and the red line represents a fit by E ~constant/r. (b) the $\frac{\mathrm{d}I}{\mathrm{d}V}$ spectra taken at different locations on the MTB as indicated, showing the peak energy shift with STM tip position.

Figure. 6. Charge Density Modulations in MTBs. (a) Room-temperature STM image (sample bias: +0.5V) of a $MoSe_2$ monolayer grown on HOPG substrate. (b) Main: STM image showing an isolated MTB on HOPG substrate (size: 20 × 20 nm^2, sample bias: −1V). Inset: Line profile of the intensity modulations along the marked line. Red curve is a plot of the $\rho \sim x^{-K_C}$ relation with K_C = 0.28. (c) Main: STM image of an MTB triangle on Au(110) substrate (size: 20 × 20 nm^2, sample bias: +0.1V). Inset: Line profile of the intensity modulation along one segment of the MTB as marked by the thin line. Red curve shows the $\rho \sim 1/x$ relation.

Figure 1

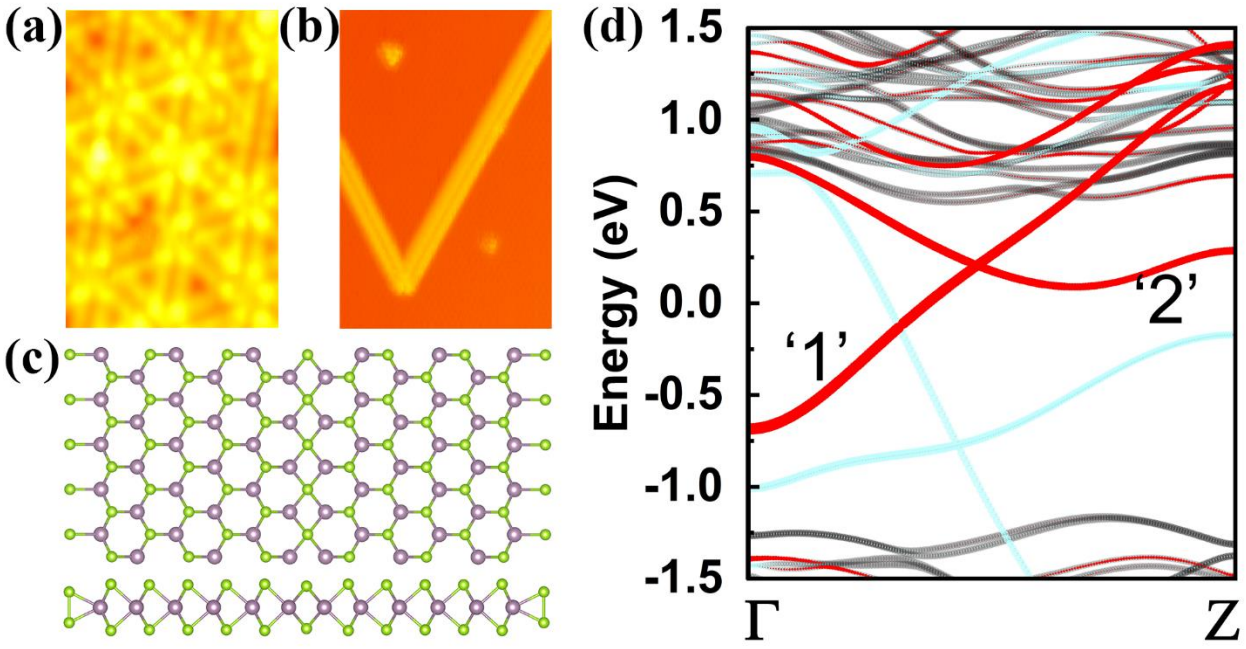

Figure 2

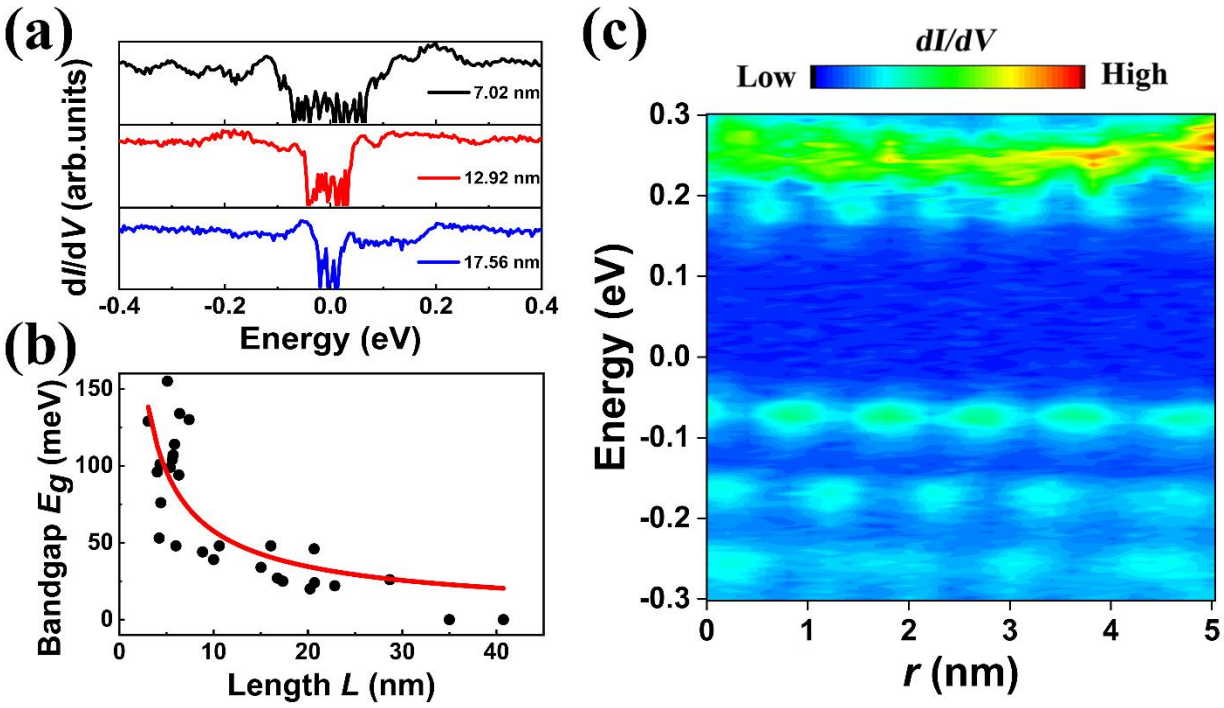

Figure 3

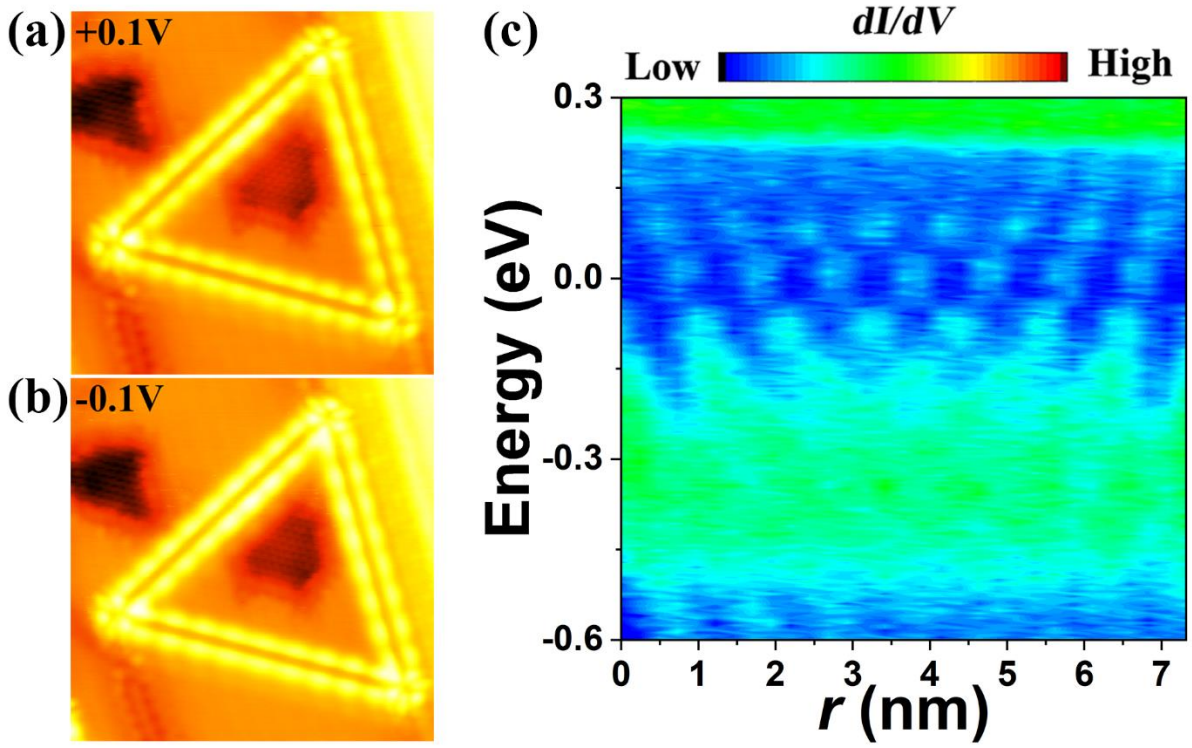

Figure 4

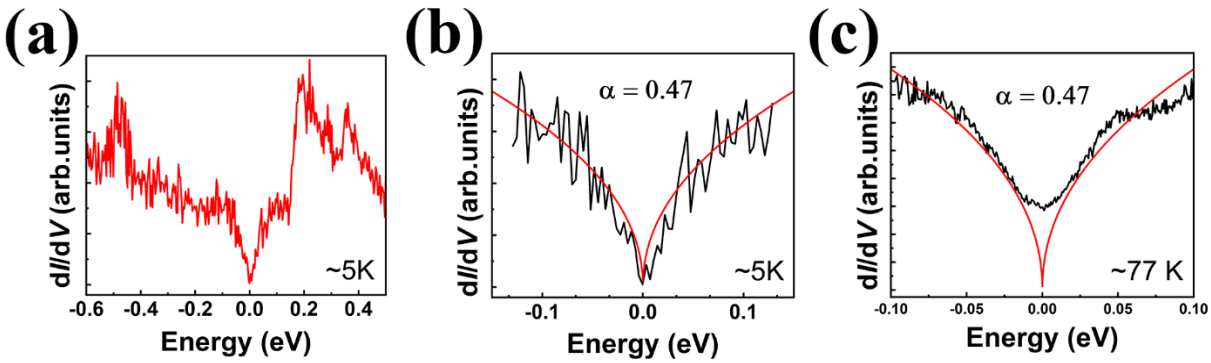

Figure 5

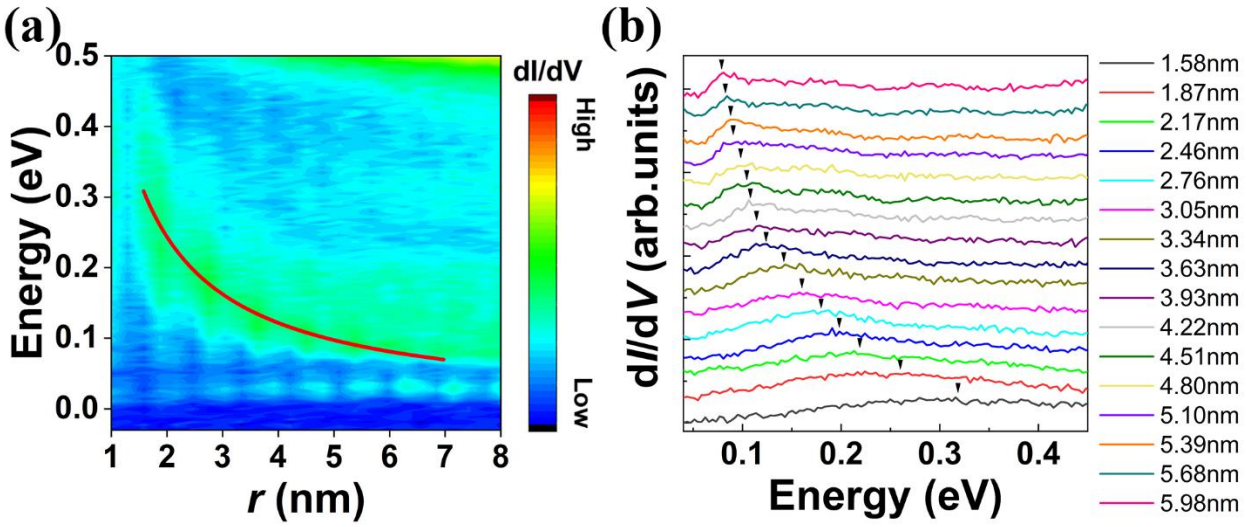

Figure 6